

Materials Technology
Advanced Performance Materials

ISSN: (Print) (Online) Journal homepage: https://www.tandfonline.com/loi/ymte20

Effect of the *Juglans Regia* (Walnut) leaf extract concentration on the biosynthesis of ZnO nanoparticles: Characterisation and antimicrobial activity

Eda Çinar Avar, Kübra Erkan Türkmen, Elif Loğoğlu & Hikmet Katircioğlu

To cite this article: Eda Çinar Avar, Kübra Erkan Türkmen, Elif Loğoğlu & Hikmet Katircioğlu (2022): Effect of the *Juglans Regia* (Walnut) leaf extract concentration on the biosynthesis of ZnO nanoparticles: Characterisation and antimicrobial activity, Materials Technology, DOI: 10.1080/10667857.2022.2136556

To link to this article: https://doi.org/10.1080/10667857.2022.2136556

Published online: 19 Oct 2022.

Submit your article to this journal

Article views: 4

View related articles

View Crossmark data

Full Terms & Conditions of access and use can be found at
https://www.tandfonline.com/action/journalInformation?journalCode=ymte20

MATERIALS TECHNOLOGY
https://doi.org/10.1080/10667857.2022.2136556

Taylor & Francis
Taylor & Francis Group

Check for updates

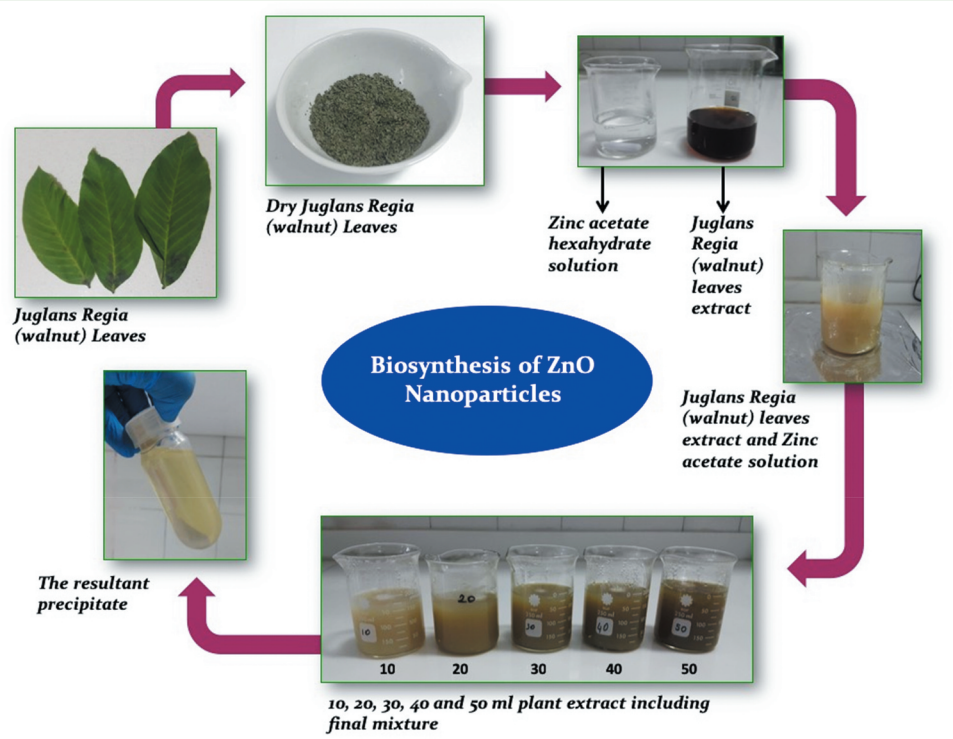
Effect of the *Juglans Regia* (Walnut) leaf extract concentration on the biosynthesis of ZnO nanoparticles: Characterisation and antimicrobial activity

Eda Çinar Avar[a*] Kübra Erkan Türkmen[b], Elif Loğoğlu[a] and Hikmet Katircioğlu[c]

[a]Department of Chemistry, Gazi University, Ankara, Turkey; [b]Department of Biology, Karamanoglu Mehmetbey University, Karaman, Turkey; [c]Department of Biology Education, Gazi University, Ankara, Turkey

ABSTRACT

In the present article, we have developed an eco-friendly, phytosynthetic, cost-effective, and straightforward method for the synthesis of ZnO nanoparticles using leaf extracts of *Juglans Regia* (JR) as green reducing agents. The powder X-ray diffraction pattern revealed the high crystalline nature of synthesised ZnO nanoparticles also rivalled with ICSD no. 98–009-4004. The SEM images of the samples showed the spherical and irregularly distributed rod and plate-like structures. The EDS spectrum filed only Zn and O peaks revealed that the sample has good purity in ZnO nanoparticles. The HRTEM analysis explained the formed ZnO nanoparticles by biogenic reduction were hexagonal shape with definite edges and the average grain size was obtained as 33.18 ± 6.2 nm for the 50JR sample. The d-spacings of fringes and SAED pattern got also rivalled with XRD d-spacings. According to the UV-Visible analysis, the values of peak absorbance wavelength decreased (blue shift) with the increase in the leaf extract concentrations. The bandgap values were calculated in the range of 2.74–3.17 eV. The Fourier Transform Infra-Red study explicated the biomolecules for the reduction of nanoparticles and also ZnO bonding. These results also proved the presence of ZnO nanoparticles synthesised using *Juglans Regia* extract. Regarding the antimicrobial effects of ZnO NPs, ZnO NP which was using 50 mL JR extracts was detected as highly efficient nanoparticles against test microorganisms. In particular, the highest antimicrobial activity was measured with 15.66 ± 1.15 mm against *Candida albicans* 10,231 and revealed data compared with fluconazole, as reference antifungal, recorded 69% antimicrobial index. The findings demonstrated that ZnO NPs can be evaluated for use in biomedical applications.



ARTICLE HISTORY
Received 27 December 2021
Revised 8 October 2022
Accepted 11 October 2022

KEYWORDS
ZnO nanoparticles; green synthesis; antimicrobial activity; Juglans regia; biosynthesis

CONTACT Eda Çinar Avar edaavar@gazi.edu.tr Department of Chemistry, Gazi University, Karaman, 06560 Ankara, Turkey
*These authors contributed equally to this work.
This article has been corrected with minor changes. These changes do not impact the academic content of the article.
© 2022 Informa UK Limited, trading as Taylor & Francis Group

Introduction

Metal oxides have been used for different purposes all over the world since ancient times [1]. Metal oxide nanoparticles are widely used in many different fields such as agriculture, textile, pharmaceutical, biomedical, energy, food, and consumer goods production [2–4]. Many metal oxide nanoparticles have a wide application area, especially in the biomedical field, due to their high stability, easy processing, preparation in the desired morphology, being easily modified with various molecules, and being biocompatible [1–4]. Since ZnO nanoparticles are chemically stable, non-toxic, and biocompatible, their use in biomedicine, tissue engineering, medicine, and cosmetics has recently attracted attention [5–10].

Zinc oxide (ZnO) nanoparticles, which are among the inorganic nanoparticles, have a wide range of applications in the plastic, glass, ceramic, rubber, cement, and food industries due to their easy processing and low cost [1,11,12]. According to their intended use, there are various physical and chemical methods for synthesising ZnO nanoparticles with targeted properties [13]. These methods are sol-gel, microwave-assisted synthesis, chemical vapour deposition, pulsed laser deposition, infrared irradiation, electrochemical reduction, hydrothermal synthesis, spray pyrolysis, UV light-mediated synthesis, mechanical milling, mechanochemical synthesis [14–23]. Chemical methods used in nanoparticle synthesis generally use organic solvents, and most of them are highly reactive and toxic to the environment [24]. The by-products formed at the end of chemical synthesis processes are also highly toxic, and these methods are low-efficient, require long reaction times, high energy at high temperature and pressure conditions, the use of large-volume costly equipment and equipment usage expertise [25–31].

Green synthesis is one of the methods used in nanoparticle synthesis and has been developing rapidly in recent years. Green synthesis aims to efficiently use non-toxic and biodegradable raw materials and solvents for the environment. The main purpose of green synthesis is to combat human health and environmental problems by relying on non-hazardous and biologically friendly precursors that prevent waste production, protect the yield and quality of the product [32,33]. In the biological synthesis method of nanoparticles, microorganisms, fungi, algae, and plants are used as reducing agents [34,35]. Among these organisms, plants seem to be the best candidates and are suitable for the large-scale biosynthesis of nanoparticles. The nanoparticles produced using various parts of plants are more stable and the synthesis rate is faster than microorganisms. In addition, nanoparticles produced from plant parts have greater diversity in shape and size compared to those produced by other organisms [36]. The biological activity of nanoparticles can vary depending on various variables such as size, morphology, surface chemistry, stability, and reactivity in solution [34]. The use of plant extracts for the green synthesis of nanoparticles has been considered more reliable than other methods, so nanoparticles prepared by green synthesis have a strong potential for biomedical applications. For the synthesis of metal oxide nanoparticles, parts of plants such as stems, leaves, flowers, fruits, roots, latex, seeds, and seed coats are used [37,38]. Plant extracts act as both reducing and stabilising agents in nanoparticle synthesis. Many plant species contain different types of antioxidative compounds (reducing agents) such as flavonoids, coumarins, xanthones, anthraquinones, and terpenoids [39,40]. Biomolecules (for example, enzymes, proteins, amino acids, vitamins, polysaccharides, and organic acids) that perform the bioreduction of metal nanoparticles and are found in plant extracts are not toxic to the environment and are chemically complex [41, 42]. These critical roles of plants for the production of metal nanoparticles from biological materials continue to attract the attention of researchers. In general, the biosynthesis of ZnO nanoparticles is accomplished by adding zinc nitrate or zinc acetate to a biological extract. The production of ZnO nanoparticles by green synthesis is a one-step, easy, low-energy, and low-cost, scalable process. After the reaction, this solution is subjected to heat treatment and ZnO powder is obtained [35,43,44].

Juglans regia is a deciduous temperate forest tree of the *Juglandaceae* family [45], which is widespread throughout the world [46,47]. Walnut tree leaf has long been used in the cosmetic and pharmaceutical industry [45], as well as in traditional medicine in Asia, for the treatment of various diseases [48,49]. Walnut leaf contains 3-Caffeoylquinic, 4-p-coumaroylquinic acids, 3-p-oumaroylquinic, 4-p-coumaroylquinic, malic acid, quercetin derivatives, sucrose, α-tocopherol, tocopherol isomer, and many phenolic compounds [50,51]. These bioactive components in walnut leaves are used as stabilising and reducing agents in the synthesis of inorganic metal oxide nanoparticles. The number of bioactive components in walnut leaves varies depending on climatic conditions, geographical origin, environmental, and some agricultural factors [52,53]. Juglans regia leaf contains a significant number of phenolic compounds, has strong antioxidant, antimicrobial, anticancer, and anti-inflammatory activity [48,49,54,55].

Various plants such as *Abutilon indicum* [[1-]], *Cassia fistula* [1,2], *Azadirachta Indica* [1–3], *Daphne mucronata* [1–4], *P. Roebelenii* [1–5], *Ocimum basilicum* [1–6], *Laurus nobilis* [1–7], *Citrus sinensis* [1–8], *Mussaenda frondosa* [1–9] have been used so far in the synthesis of ZnO nanoparticles. *Juglans regia* is one of

the widely cultivated tree species worldwide. The use of *Juglans regia* leaf for the synthesis of various nanoparticles will enable this low-cost product, which is abundant in nature, to be converted into functional materials. In the study by Darvishi, E et al. [1–10], ZnO nanoparticles were synthesised using *Juglans regia* leaf extract and various properties were compared with ZnO nanoparticles synthesised by chemical method. However, to the best of our knowledge, ZnO nanoparticle synthesis using different amounts of *Juglans regia* leaf extract has not been studied before. This study aims to investigate the structural and morphological changes of ZnO nanoparticles and antimicrobial activity changes against various microorganisms by changing the *Juglans Regia* (walnut) leaf extract concentration. Characterisations of ZnO NPs were done by using XRD, SEM, EDS, HRTEM, UV-VIS, FT-IR, and TG. Antimicrobial activities of ZnO nanoparticles were evaluated using standard test microorganisms (*Pseudomonas aeruginosa* RSKK 07031 B9, *Escherichia coli* RSKK 97021, *Bacillus cereus* RSKK 05915, *Staphylococcus aureus* RSKK 96045, *Candida albicans* ATCC 10231).

Experimental procedure

Chemical and reagents

The *Juglans regia* (walnut) leaves were collected from Gezin Station Village, Maden, Elazığ, Turkey. Zinc acetate hexahydrate (Zn $(CH_3COO)_2.6H_2O$), dimethyl sulphoxide (DMSO), Mueller-Hinton Agar (MHA), Nutrient Broth (NB), Sabouraud Dextrose Broth (SDB), and Sabouraud Dextrose Agar (SDA) were purchased from Merck (Merck Co., Darmstadt, Germany). All the chemicals used were of analytical grade and without any additional purification steps.

Preparation of Juglans regia leaves extracts

Juglans regia leaves were thoroughly washed with tap water and dried at room temperature in dust-free condition. Dried leaves were crushed into the finest powder. 25 g of the powder was boiled with 250 mL of deionised water at 75°C for 30 min. After two hours, the aqueous leaves were extracted by filtration (Whatman No. 1) filter paper and the resulting filtrate was stored at 4°C for further use.

Biosynthesis of ZnO nanoparticles

For ZnO nanoparticles biosynthesis, 0.2 M zinc acetate hexahydrate was mixed with 10, 20, 30, 40, 50 mL of the extract under vigorous stirring for two hours. After the completion of the reaction, the precipitate was separated from the reaction solution by centrifugation at10000rpm for 10 min. The resultant precipitate was washed repeatedly with double distilled water followed by ethanol to remove the impurities. Finally, a solid white powder was obtained after overnight drying of the purified precipitate at 60°C in an oven. The powder was then subjected to calcination under a muffle furnace at 400°C for 2 h. The obtained dried particles were collected and used for further characterisation studies.

Characterisation of ZnO nanoparticles

X-Ray Diffraction (XRD) Analysis of ZnO Nanoparticles

The crystalline nature of the synthesised ZnO nanoparticles was characterised by Panalytical Empyrean XRD with Cu Kα radiation (λ = 1.154 Å), accelerating voltage 45 kV, beam current 40 mA, in an angular range of 10–80° at a step size of 0.02° and a counting time of 1 s. The estimation of the sizes of particles was performed by Debye–Scherrer's formula.

Scanning electron microscopy and energy dispersive X-ray analysis (SEM-EDS)

The morphological characterisation of the ZnO nanoparticles was carried out using FEI Quanta FEG 450 SEM at 10 kV in secondary electron mode. The elemental presence of zinc oxide was confirmed with EDX analysis using Bruker Quantax 200 EDX detector.

High-resolution transmission electron microscopic (HRTEM) Analysis

The synthesised ZnO nanoparticles were characterised for their shape and size distribution using a Transmission electron microscope (TEM, TECNAI G2 F-30, FEI). The structural characterisation and particle size examination of zinc oxide nanoparticles were carried out by Transmission Electron Microscopy (TEM) (JEM-1230, JEOL, Akishima, Japan). The samples were put on the carbon-coated copper grid for 1 min to make a small film of the sample. The excess liquid was removed with a filter paper, and it was then set in a grid box sequentially.

UV–Vis spectroscopy analysis

The synthesised ZnO nanoparticles were characterised with UV-Vis spectroscopy by measuring the absorbance between the spectrum range of 300–700 nm.

Fourier transform infrared spectroscopic (FT-IR) analysis

The ZnO nanoparticles were analysed to determine the functional groups present by Fourier transform

infrared spectroscopy (FTIR). The analysis was done using a Thermo Nicolet Smart Golden Gate MKII spectrometer equipped with a single reflection ATR and further measurements were recorded at a scan range of 400–4000 cm^{-1} at room temperature.

Thermogravimetric (TG) analysis

The thermal behaviour of the NPs was investigated from 50°C to 1000°C with a heating rate of 20°C/min by SII Exstar TG/DTA 7200 in a flowing N_2 atmosphere.

Antimicrobial activity of ZnO nanoparticles

Antimicrobial activity of the ZnO nanoparticles was examined by the disc diffusion method Gram-positive bacteria (*B. cereus* RSKK 05915, *S. aureus* RSKK 96045) and Gram-negative bacteria (*P. aeruginosa* RSKK 07031 B9, *E. coli* RSKK 97021) and yeast (*C. albicans* ATCC 10231). Bacterial cultures were taken into the Nutrient Broth medium before antibacterial testing and refreshed in a shaking incubator at 37°C for 24 h. The turbidity of the bacterial cultures was then adjusted to 0.5 McFarland standard. A 100 µL of appropriate dilution (~10^6 CFU/mL) of bacterial culture was seeded by spread plate technique on sterile MHA plates. Yeast strain (*C.albicans* 10,231) was grown into SDB medium at 37°C for 24 h. Then culture was diluted for arranging turbidity as 0.5 McFarland standard. 100 µL of fresh yeast culture was spread onto the SDA medium. All ZnO NPs were dissolved in DMSO to adjust a final concentration of 5 mg/mL and filtered through 0.2 µm Sartorius filters for sterilisation. The 6 mm sterile filter discs (Bioanalyse, Turkey) were placed on MHA (for bacterial strains) and SDA (for yeast) plates at appropriate distances, then 20 µL of samples were impregnated to each disc. The plates were incubated at 37°C for 24 h, then the zone of inhibition was measured in millimetres. All tests were performed in three replicates and the inhibition zones were compared with reference antibiotic – antibacterial Chloramphenicol (30 µg, Oxoid antibiotic disc, Germany) and antifungal – Fluconazole (25 µg, Oxoid antibiotic disc, Germany). The antimicrobial index was calculated using the formula below.

[56].

Antimicrobial index: (ZnO-NPs inhibition zone/ antibiotic inhibition zone) x 100

Results and discussions

X-Ray Diffraction (XRD) Analysis of ZnO-NPs

To understand the crystal structure and phase purity of the ZnO samples, an XRD analysis was performed. Figure 1 shows the XRD patterns of the ZnO nanoparticles at five different concentrations of *Juglans Regia* leaf extract (10, 20, 30, 40, 50 mL). The diffraction peaks for all samples detected in a range of 10–80° (2θ) were matched perfectly with the standard diffraction peaks, indexed as (100), (002), (101), (102), (110), (103), (200), (112), (201), and (202) for hexagonal structured ZnO with space group-P63mc (186) in the database (ICSD no. 98–009-4004). In addition, no impurity diffraction peaks were noticed to correspond to any other phase. This indicates obtaining the high purity of ZnO products. The crystallite size and the lattice strain of all samples were calculated based on the highest intensity peak (101) using the following Equations, respectively [57].

$$D = \frac{0.9\lambda}{\beta \cos\theta} \tag{1}$$

$$\varepsilon = \frac{\beta}{4 \tan\theta} \tag{2}$$

Here, D is the crystallite size, λ is the X-ray wavelength, β is the full width at half maximum (FWHM), θ is the Bragg diffraction angle, and ε is the lattice strain. However, the dislocation density (δ) which defines the number of defects in the samples were calculated from the following equation [57].

$$\delta = \frac{1}{D^2} \tag{3}$$

For the different concentrations of *Juglans Regia* leaf extract, the obtained structural values are listed in Table 1. It can be observed that the crystallite size values have a reduction with the increasing concentration of the leaf extract, which is similar to the works by Miri et al. [58]. The crystallite sizes of all samples were obtained between 232.2 and 41.4 nm. Conversely, the

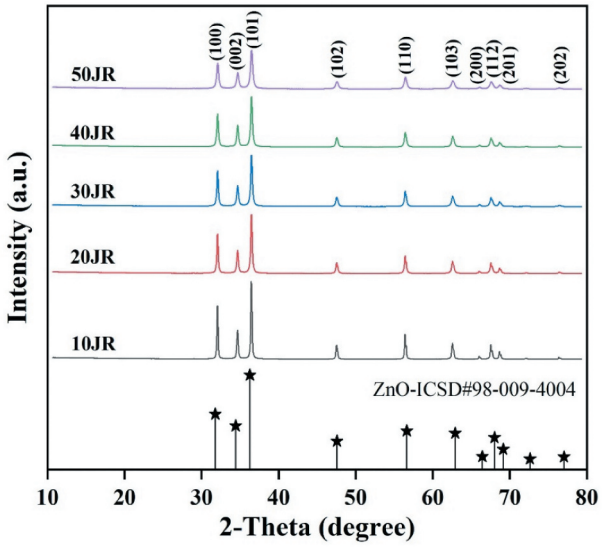


Figure 1. XRD patterns of the ZnO nanoparticles synthesised using different concentrations of *Juglans Regia* leaf extract.

Table 1. Microstructural parameters were obtained from the XRD analysis of ZnO nanoparticles.

Sample code	2θ (101) (°)	FWHM (°)	D (nm)	ε (%)	δ x 10^{-4} (nm^{-2})	a = b (nm)	c (nm)	V (nm^3)	L (nm)
10JR	36.2926	0.1363	232.2	0.123	0.185	0.3245	0.5203	0.0474	0.1975
20JR	36.2997	0.1733	114.1	0.188	0.768	0.3245	0.5202	0.0474	0.1975
30JR	36.3049	0.2090	76.7	0.244	1.699	0.3244	0.5202	0.0474	0.1975
40JR	36.3063	0.2247	67.0	0.268	2.227	0.3244	0.5201	0.0474	0.1974
50JR	36.3145	0.3020	41.4	0.379	5.834	0.3243	0.5201	0.0473	0.1974

lattice strains and dislocation densities increased with the crystallise size reduction. The maximum lattice strain of 0.379% and the maximum dislocation density of 5.834×10^{-4} nm^{-2} were observed for the 50 mL of leaf extract. These results indicated that because of the grain boundary effect the small crystallite size was induced by the large lattice strain and imperfections might be produced by a relative displacement between the lattices [59]. The lattice parameters such as *a, c*, and volume of the unit cell (*V*) of all samples were estimated by using the three major peaks corresponding to (100), (002), and (101) planes, and calculated the following Equations [60].

$$\sin^2\theta = \frac{\lambda^2}{4}\left[\frac{4}{3}\left(\frac{h^2+hk+k^2}{a^2}+\frac{l^2}{c^2}\right)\right] \quad (4)$$

$$V = 0.866a^2c \quad (5)$$

As seen from Table 1, the calculated lattice parameters were almost unchanged with the concentration of the leaf extract. Concerning this, the constant value (*c/a*) was 1.603 for all samples and found that it is in good agreement with the ICSD data (#94004). In addition, the Zn-O bond length (*L*) was calculated by using the following Equation [61];

$$L = \left[\frac{a^2}{3}+c^2(0.5-u)^2\right]^{0.5} \quad (6)$$

where *u* is the internal positional parameter, and can be obtained from the following Equation [61].

$$u = \frac{1}{2}\left(\frac{a}{c}\right)^2+\frac{1}{4} \quad (7)$$

Since there is a correlation between *c/a* and *u* parameters, the *u* parameter was found to be equal to 0.3796 for all samples. As seen in Table 1, the bond length between Zn and O remained nearly constant, whereas the Zn-O bond length of pure ZnO nanoparticles was reported as 0.19752 nm [62].

Scanning electron microscopy and energy dispersive X-ray analysis (SEM-EDS)

The particle morphology and the chemical composition of all the samples were examined by SEM and EDS analyses, as shown in Figure 2. The SEM images at low and high magnifications (10kX, left side and 100kX, middle side) displayed apparent morphological changes in response to various concentrations of the leaf extract. The investigated particles by SEM were seemed to be composed of almost spherical and irregularly distributed rod and plate-like structures with an agglomerated morphology. The polarity and electrostatic attraction of the ZnO nanoparticles might be the reason for this observed agglomeration, as reported in the previous study [63]. However, the EDS spectra on the right side of Figure 2 revealed that all structures consist of just Zn and O elements, where the peaks are located at around 1.01, 8.64, and 9.60 eV for zinc, and peaks located at around 0.52 keV for oxygen. This confirms the purity of the synthesised nanoparticles, which agrees well with the XRD results. In addition, almost all the samples showed a similar chemical composition to the theoretically expected stoichiometric mass percentage of Zn as 80.3% and the O as 19.7% [63].

Transmission electron microscope (TEM) analysis

Figure 3 shows the TEM analysis results for the 50 mL of leaf extract. The bright field TEM image in Figure 3a exhibited the presence of almost spherical and partly hexagonal-shaped ZnO nanoparticles with an agglomerated morphology. As shown in Figure 3b, the average grain size distribution of the sample 50JR is 33.18 ± 6.2 nm. Similar morphology and size distribution were reported by Soares et al. [64] and Dinca et al. [65]. However, the spacing between the lattice fringes was obtained from the high-resolution TEM (HRTEM) image of the sample (Figure 3c). The lattice fringe values were measured to be around 0.28 nm and 0.24 nm, which are consistent with (100) and (101) planes of ZnO, respectively. The selected area electron diffraction (SAED) ring pattern (Figure 3d) also confirms the polycrystalline nature of the sample and agrees with the XRD analysis.

UV–vis spectral analysis of synthesised ZnO-NPs

UV–Vis absorbance spectra of the ZnO nanoparticles measured at room temperature are presented in Figure 4. As seen from the spectra, the excitonic absorption peaks of the nanoparticles are located at around 380, 375, 372, 371, and 369 nm for 10JR, 20JR, 30JR, 40JR, and 50JR samples, respectively. This is ascribed to the transition of electrons from the valence band to the conduction band [66, 67]. However, the values of peak absorbance wavelength

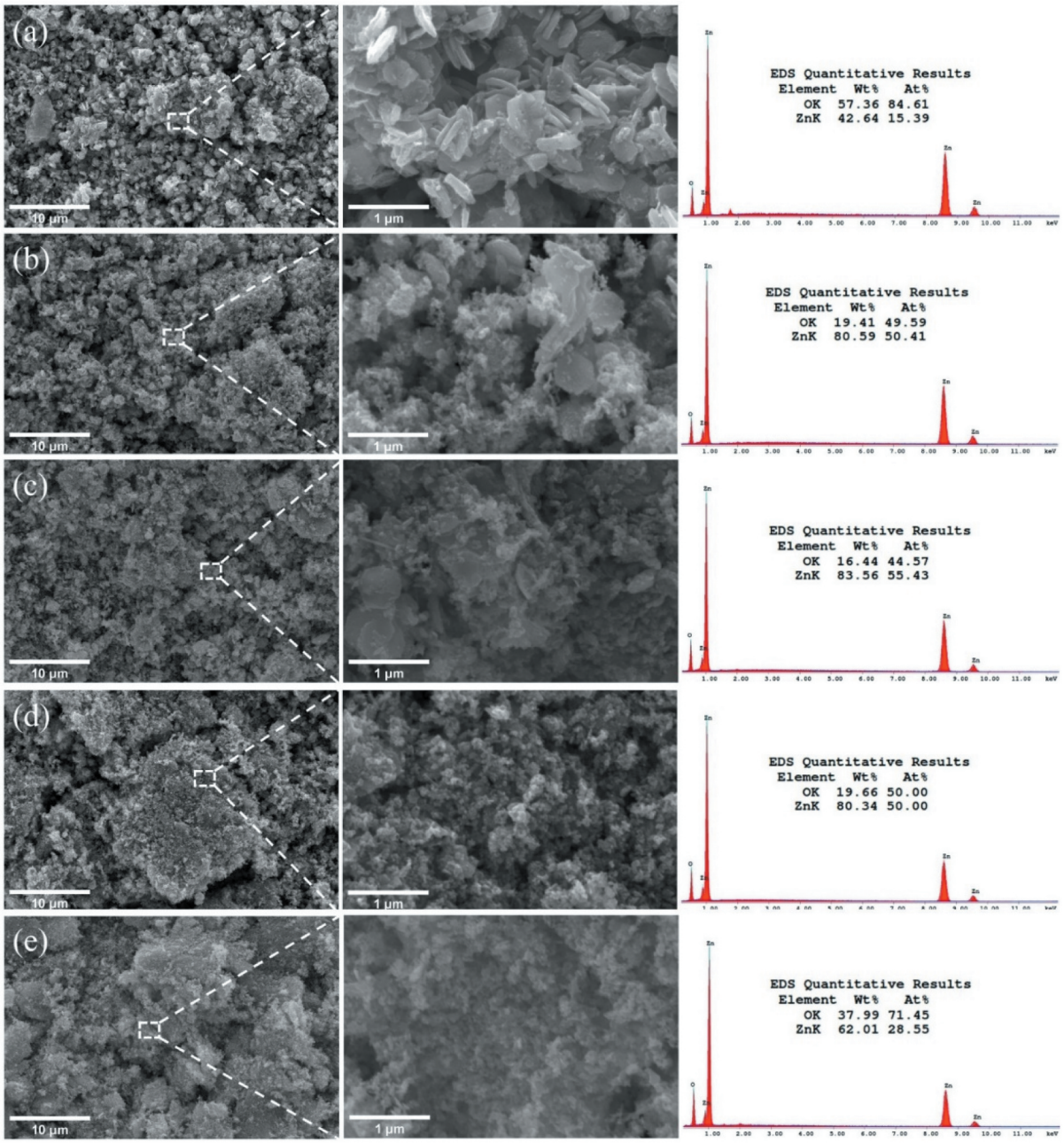


Figure 2. Low and high magnification SEM images and corresponding EDX spectra of the synthesised ZnO nanoparticles using different concentrations of *Juglans Regia* leaf extract; (a) 10JR, (b) 20JR, (c) 30JR, (d) 40JR, and (e) 50JR mL.

decreased (blue shift) with the increase in the leaf extract concentrations. This shift in the peaks may be due to the changes in size, shape, and surface microstructures [66]. Also, it should be mentioned that there is an inverse proportion between the absorbance wavelength and the bandgap energy related to the size effect [63]. The direct bandgap energy of the samples was estimated by using the Kubelka–Munk relation [68]. As shown inset in Figure 4, the bandgap values of the 10JR, 20JR, 30JR, 40JR, and 50JR samples were found to be 2.74, 3.02, 3.09, 3.14, and 3.17 eV, respectively. This increment of the bandgap values can be attributed to the decrease in the crystallite size, as given in Table XRD.

Fourier transform infrared spectroscopic (FTIR) Analysis

To characterise the formation of functional groups on the surface of ZnO nanoparticles, the attenuated total reflection (ATR)-FTIR spectra were employed. As seen in Figure 5, the ZnO nanoparticles synthesised using different concentrations of the leaf extract consist of several functional groups. The broad peaks between the range of 3200–3700 cm^{-1} correspond to O-H stretching due to the presence of water molecules absorbed by the ZnO nanoparticles. The peaks at around 2800–2900 cm^{-1} represent the C-H stretching vibrations. The functional group of CO_2 at around 2300 cm^{-1} wavenumber could arise from ambient air. However, the peaks at around

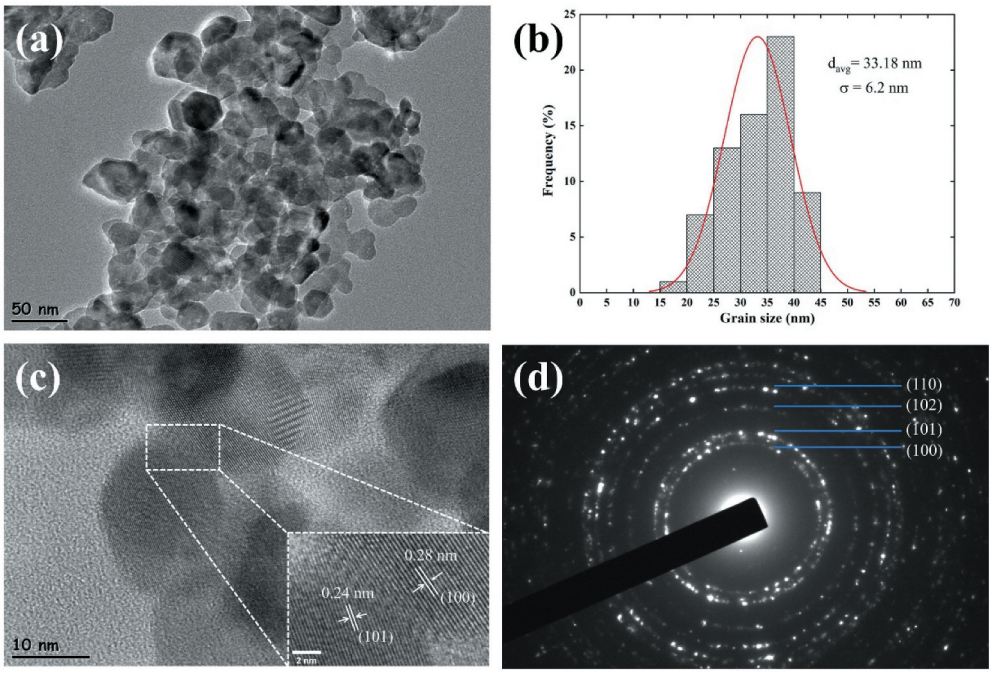


Figure 3. (a) TEM image, (b) its corresponding size distribution, (c) HRTEM image, and (d) corresponding SAED pattern of the sample 50JR.

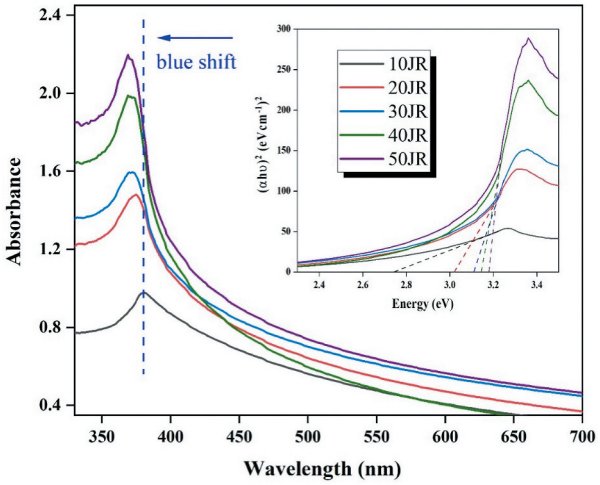


Figure 4. UV-Vis absorption spectra of the synthesised ZnO nanoparticles using different concentrations of *Juglans Regia* leaf extract. The inset represents the bandgap energy of the samples.

1050, 1350, 1550 cm^{-1} can be attributed to the stretching modes of the C-C, C-H, and C = O, respectively. At the low-wavenumber region, the peaks between 700 and 900 cm^{-1} and 400–600 cm^{-1} indicate the Zn-OH and Zn-O vibrations, respectively. These results are in good agreement with the observed functional groups of ZnO in previous studies [52,69,70, 71].

Thermogravimetric (TG)-Differential thermal analysis (DTA) analysis

The thermogravimetric analysis (TG) curves of the synthesised ZnO nanoparticles using different concentrations of the leaf extract are shown in Figure 6. The thermal stability of the samples was explored by TG analysis at the temperature range of 25–900°C. The total weight loss was determined approximately as 1.1, 2.5, 2.7, 2.8, and 3.0% for 10JR, 20JR, 30JR, 40JR, and 50JR samples, respectively. According to the data, the weight loss of the samples increased with the increasing leaf extract concentrations. This can be attributed to the desorption of surface water and the thermal degradation of residual organics [72,73]. It can be concluded that the biosynthesis of ZnO nanoparticles demonstrated good thermal stability with slight weight loss.

Antimicrobial activity of ZnO nanoparticles

The findings obtained from the antimicrobial activity test showed that 50-JR was the most efficient ZnO NPs against test microorganisms. Data were given in Figure 7 that the antimicrobial effect of ZnO NPs had increased depending on the concentration of JR in nanoparticles.

50-JR showed that had the most efficient nanoparticle with the biggest inhibition zone value for all test microorganisms; however, *C. albicans* 10,231 displayed the biggest inhibition zone with 15,66 ± 1,15 mm. The inhibition zone for *P. aeruginosa* RSKK 07031 B9 was the second-highest inhibition zone at 50-JR with a - 12,66 ± 0,57 mm. Other results for 50-JR's antimicrobial activity detected orderly as for *S. aureus* RSKK 96045 10,33 ± 0,57 mm, *E. coli* RSKK 97021 8,33 ± 1,15 mm, *B. cereus* RSKK 05915

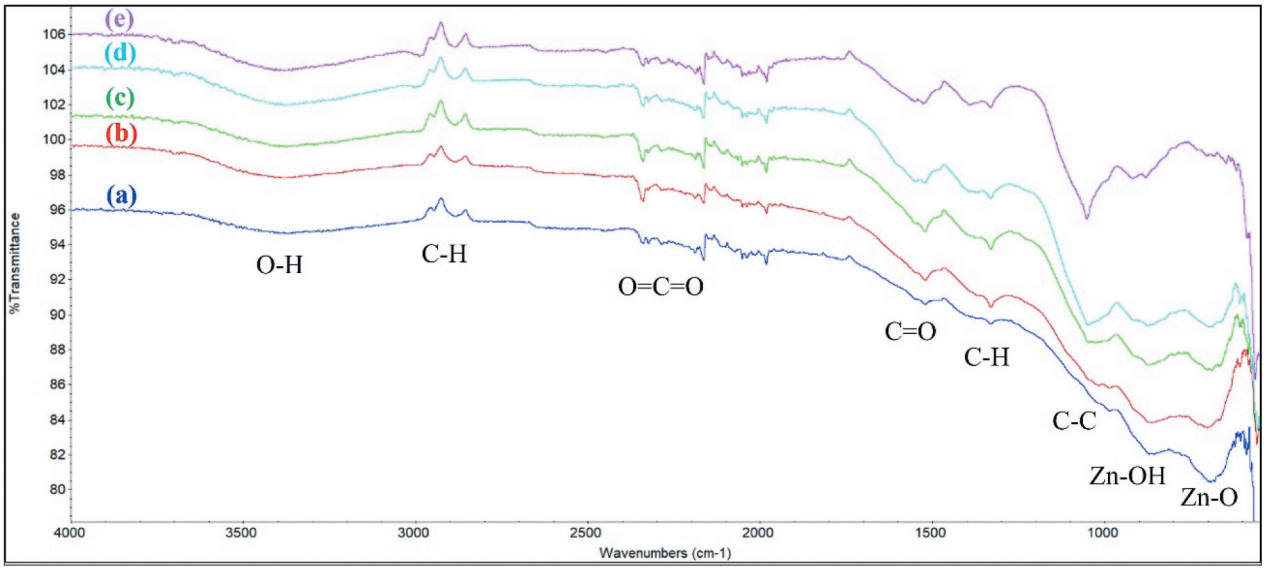


Figure 5. ATR–FTIR spectra of the synthesised ZnO nanoparticles using different concentrations of *Juglans Regia* leaf extract; (a) 10JR, (b) 20JR, (c) 30JR, (d) 40JR, and (e) 50JR mL.

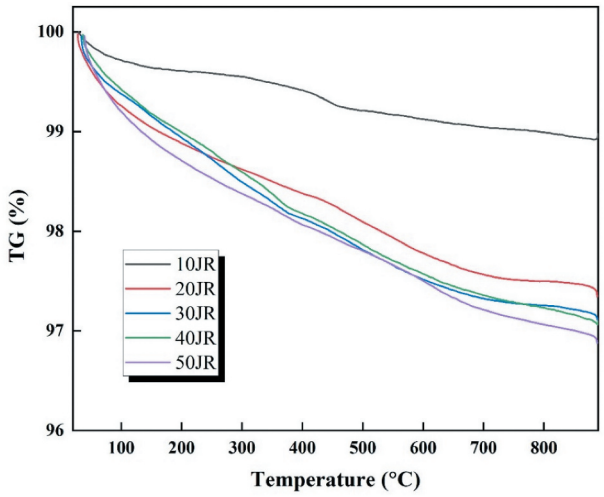


Figure 6. Weight loss curves of the ZnO nanoparticles.

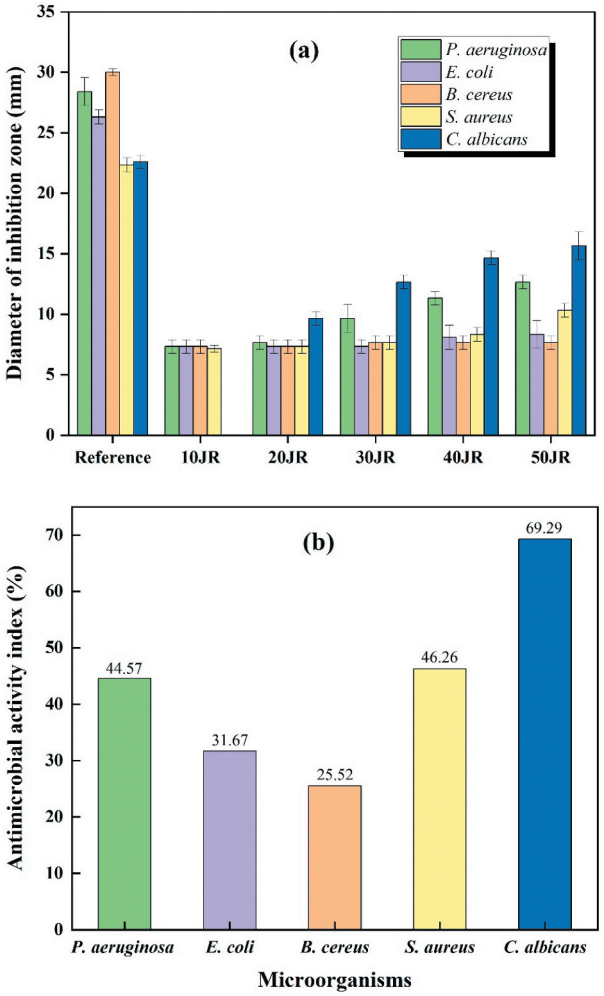


Figure 7. (a) *In vitro* antimicrobial activity of ZnO nanoparticles and (b) antimicrobial activity index against test microorganisms

7,66 ± 0,57 mm. Considering revealed outputs from 40-JR-ZnO, 30-JR, 20-JR, and 10-JR antimicrobial activity results decreased from 50-JR to 10-JR as seen in Fig.7. To compare the reference antibiotic/antifungal results with ZnO NPs which were selected only as highly efficient ZnO NP (50-JR), the antimicrobial index was calculated and have shown in Fig.7. When literature evaluated for comparing antimicrobial results of ZnO NPs, antimicrobial activity of ZnO NPs have various effects depending on synthesis material (plant material, etc.) or applied concentrations. Some of these studies showed green- synthesis ZnO NPs had an antimicrobial effect on different Gram-negative, Gram-positive bacteria, and yeast. One of these studies carried out by Gupta et. al which was used green synthesised ZnO NPs with leaf extract of *Catharanthus roseus*, against *P. aeruginosa* MTCC 424, *E. coli* MTCC 40, *S. aureus* MTCC 9760, and the antibacterial inhibition zones were found between 11.09 ± 0.01 and 11.74 ± 0.03 mm [74]. Besides, in an experiment conducted by M. Jalal et. al was determined that

anticandidal activity by bioinspired ZnO NPs, synthesised by using leaf extract of *Crinum latifolium*, against *Candida* species [75]. Additionally, the index value for the reference antifungal fluconazole used for *C. albicans* ATCC 10231 was determined as 69% and was considered remarkable for biomedical applications. Antifungal activity mechanism of ZnO NPs demonstrated by M.Jalal et. Al [75], Shoeb et. Al [76] and was stated that exposure of ZnO enhanced reactive oxygen species (ROS). Here, our results exhibited that JR-NPs possessed antimicrobial potential against gram-negative, gram-positive bacteria and yeast. In particular, antifungal activity on *C. albicans* 10,231 draws attention with the highest inhibition compared to the other bacteria.

Conclusions

In the biomedical field, nanoparticles are used as antimicrobial, anticancer, and anti-inflammatory agents. As metal oxide nanoparticles continue to be researched, their usage areas are also expanding. In this study, ZnO nanoparticle was synthesised by green synthesis method using walnut leaf extract, which is inexpensive, non-toxic, short time, and does not require much energy, and environmentally friendly green synthesis method. The effect of varying extract amounts on the structural, morphological, and antimicrobial properties of the synthesised ZnO nanoparticle was investigated. It has been determined that the green synthesised ZnO nanoparticles decreased the particle size and showed better antimicrobial activity as the amount of extract used increased.

Acknowledgments

HRTEM analyzes were performed in the central laboratories of the Middle East Technical University (METU).

Disclosure statement

No potential conflict of interest was reported by the author(s).

References

[1] Velsankar K, Sudhahar S, Parvathy G, et al. Effect of cytotoxicity and antibacterial activity of biosynthesis of ZnO hexagonal-shaped nanoparticles by Echinochloa frumentacea grains extract as a reducing agent. Mater Chem Phys. 2020;239:121976.
[2] Nikolova MP, Chavali MS. Metal oxide nanoparticles as biomedical materials. Biomimetics. 2020;5(2):27.
[3] Chan YY, Pang YL, Lim S, et al. Facile green synthesis of ZnO nanoparticles using natural-based materials: properties, mechanism, surface modification, and application. J Environ Chem Eng. 2021;9(4):105417.
[4] Aldeen TS, Mohamed HE, Maaza M. ZnO nanoparticles prepared via a green synthesis approach: physical properties, photocatalytic and antibacterial activity. J Phys Chem Solids. 2022;160:110313.
[5] Deng Z, Chen M, Gu G, et al. A facile method to fabricate ZnO hollow spheres and their photocatalytic property. J Phys Chem B. 2008;112(1):16–22.
[6] Krishnakumar T, Jayaprakash R, Pinna N, et al. Microwave-assisted synthesis and characterization of flower-shaped zinc oxide nanostructures. Mater Lett. 2009;63(2):242–245.
[7] Cao B, Cai W. From ZnO nanorods to nanoplates: chemical bath deposition growth and surface-related emissions. J Phys Chem C. 2008;112(3):680–685.
[8] Khatamian M, Divband B, Jodaei A. Degradation of 4-nitrophenol (4-NP) using ZnO nanoparticles supported on zeolites and modeling of experimental results by artificial neural networks. Mater Chem Phys. 2012;134(1):31–37.
[9] Khatamian M, Khandar AA, Divband B, et al. Heterogeneous photocatalytic degradation of 4-nitrophenol in aqueous suspension by Ln (La3+, Nd3+ or Sm3+) doped ZnO nanoparticles. J Mol Catal A Chem. 2012;365:120–127.
[10] Divband B, Khatamian M, Eslamian GK, et al. Synthesis of Ag/ZnO nanostructures by different methods and investigation of their photocatalytic efficiency for 4-nitrophenol degradation. Appl Surf Sci. 2013;284:80–86.
[11] Ma H, Williams PL, Diamond SA. Ecotoxicity of manufactured ZnO nanoparticles–a review. Environ Pollut. 2013;172:76–85.
[12] Wang D, Cui L, Chang X, et al. Biosynthesis and characterization of zinc oxide nanoparticles from Artemisia annua and investigate their effect on proliferation, osteogenic differentiation, and mineralization in human osteoblast-like MG-63 cells. J Photochem Photobiol. 2020;202:111652.
[13] Verma R, Pathak S, Srivastava AK, et al. ZnO Nanomaterials: green synthesis, toxicity evaluation and new insights in biomedical applications. J Alloy Comd. 2021; 876: 160175.
[14] Ikhmayies SJ. Synthesis of ZnO microrods by the spray pyrolysis technique. J Electron Mater. 2016;45 (8):3964–3969.
[15] Skoda D, Urbanek P, Sevcik J, et al. Microwave-assisted synthesis of colloidal ZnO nanocrystals and their utilization in improving polymer light-emitting diodes efficiency. Mater Sci Eng B. 2018;232:22–32.
[16] Khan MF, Ansari AH, Hameedullah M, et al. Sol-gel synthesis of thorn-like ZnO nanoparticles endorsing mechanical stirring effect and their antimicrobial activities: potential role as nano-antibiotics. Sci Rep. 2016;6(1):1–2.
[17] Manikandan E, Kavitha G, Kennedy J. Epitaxial zinc oxide, graphene oxide composite thin films by laser technique for micro-Raman and enhanced field emission study. Ceram Int. 2014;40(10):16065–16070.
[18] Parveen K, Banse V, Ledwani L. Green synthesis of nanoparticles: their advantages and disadvantages. AIP Conf Proc. 2016;1724:020048.
[19] Hoseini SJ, Darroudi M, Oskuee RK, et al. Honey-based synthesis of ZnO nanopowders and their cytotoxicity effects. Adv Powder Technol. 2015;26 (3):991–996.
[20] Hadia NM, García-Granda S, García JR. Effect of the temperature on structural and optical properties of

zinc oxide nanoparticles. J Nanosci Nanotechnol. 2014;14(7):5443–5448.
[21] Suntako R. Effect of zinc oxide nanoparticles synthesized by a precipitation method on mechanical and morphological properties of the CR foam. Bull Mater Sci. 2015;38(4):1033–1038.
[22] Kumar PN, Sakthivel K, Balasubramanian V. Microwave-assisted biosynthesis of rice-shaped ZnO nanoparticles using Amorphophallus konjac tuber extract and its application in dye-sensitized solar cells. Mater Sci Pol. 2017;35:111–119.
[23] Pathania D, Kumari M, Gupta VK. Fabrication of ZnS–cellulose nanocomposite for drug delivery, antibacterial and photocatalytic activity. Mater Des. 2015;87:1056–1064.
[24] Kaminska I, Fronc K, Sikora B, et al. Synthesis of ZnA 2 O 4:(Er 3+,Yb 3+) spinel-type nanocrystalline upconverting luminescent marker in HeLa carcinoma cells, using a combustion aerosol method route. RSC Adv. 2014;4(100):56596–56604.
[25] Saravanan K, Suriakarthick R, Ananthakumar S, et al. Colloidal synthesis of copper cadmium sulfide (CuCdS2) nanoparticles and its structural, optical, and morphological properties. Mater Sci Semicond Process. 2017;66:123–130.
[26] Biao L, Tan S, Wang Y, et al. Synthesis, characterization and antibacterial study on the chitosan-functionalized Ag nanoparticles. Mater Sci Eng C. 2017;76:73–80.
[27] Bandeira M, Giovanela M, Roesch-Ely M, et al. Green synthesis of zinc oxide nanoparticles: a review of the synthesis methodology and mechanism of formation. Sustain Chem Pharm. 2020;15:100223.
[28] Thi TU, Nguyen TT, Thi YD, et al. Green synthesis of ZnO nanoparticles using Orange fruit peel extract for antibacterial activities. RSC Adv. 2020;10 (40):23899–23907.
[29] Verma R, Gangwar J, Srivastava AK. Multiphase TiO 2 nanostructures: a review of efficient synthesis, growth mechanism, probing capabilities, and applications in bio-safety and health. RSC Adv. 2017;7 (70):44199–44224.
[30] Kumar P, Khanduri H, Pathak S, et al. Temperature selectivity for single-phase hydrothermal synthesis of PEG-400 coated magnetite nanoparticles. Dalton Trans. 2020;49(25):8672–8683.
[31] Pathak S, Jain K, Kumar P, et al. Improved thermal performance of annular fin-shell tube storage system using magnetic fluid. Appl Energy. 2019;239:1524–1535.
[32] Duan H, Wang D, Li Y. Green chemistry for nanoparticle synthesis. Chem Soc Rev. 2015;44 (16):5778–5792.
[33] Vijayaraghavan K, Ashokkumar T. Plant-mediated biosynthesis of metallic nanoparticles: a review of literature, factors affecting synthesis, characterization techniques and applications. J Environ Chem Eng. 2017;5(5):4866–4883.
[34] Kharissova OV, Dias HR, Kharisov BI, et al. The greener synthesis of nanoparticles. Trends Biotechnol. 2013;31(4):240–248.
[35] Król A, Pomastowski P, Rafińska K, et al. Zinc oxide nanoparticles: synthesis, antiseptic activity, and toxicity mechanism. Adv Colloid Interface Sci. 2017;249:37–52.
[36] Vijayakumar S, Vaseeharan B, Malaikozhundan B, et al. Laurus nobilis leaf extract mediated green synthesis of ZnO nanoparticles: characterization and biomedical applications. Biomed Pharmacother. 2016;84:1213–1222.
[37] Singh J, Dutta T, Kim KH, et al. 'Green'synthesis of metals and their oxide nanoparticles: applications for environmental remediation. J Nanobiotechnol. 2018;16(1):1–24.
[38] Malaikozhundan B, Vinodhini J. Nanopesticidal effects of Pongamia pinnata leaf extract coated zinc oxide nanoparticle against the Pulse beetle, Callosobruchus maculatus. Mater Today Commun. 2018;14:106–115.
[39] Doble M, Rollins K, Kumar A. Green Chemistry and Engineering. 1st ed. Cambridge: Academic Press; 2007.
[40] Auld DS. Zinc coordination sphere in biochemical zinc sites. Zinc biochemistry, physiology, and homeostasis. Biometals. 2001;14(3/4):271–313.
[41] Kuppusamy P, Yusoff MM, Maniam GP, et al. Biosynthesis of metallic nanoparticles using plant derivatives and their new avenues in pharmacological applications–An updated report. Saudi Pharm J. 2016;24(4):473–484.
[42] Król A, Pomastowski P, Rafińska K, et al. Zinc oxide nanoparticles: synthesis, antiseptic activity, and toxicity mechanism. Adv Colloid Interface Sci. 2017;249:37–52.
[43] Mirzaei H, Darroudi M. Zinc oxide nanoparticles: biological synthesis and biomedical applications. Ceram Int. 2017;43(1):907–914.
[44] Singh P, Kim YJ, Zhang D, et al. Biological synthesis of nanoparticles from plants and microorganisms. Trends Biotechnol. 2016;34(7):588–599.
[45] Tsamouris G, Hatziantoniou S, Demetzos C. Lipid analysis of Greek walnut oil (Juglans regia L.). Z Naturforsch C Biosci. 2002;57(1–2):51–56
[46] Naveed F, Ul Islam Z, Rehana R. Antibiofilm forming activity of naturally occurring compound. Biomedica. 2012;28:171–175.
[47] Alam F, Islam MA, Kamal MA, et al. Updates on managing type 2 diabetes mellitus with natural products: towards antidiabetic drug development. Curr Med Chem. 2018;25(39):5395–5431.
[48] Javidanpour S, Tabtabaei SR, Siahpoosh A, et al. Comparison of the effects of fresh leaf and peel extracts of walnut (Juglans regia L.) on blood glucose and β-cells of streptozotocin-induced diabetic rats. Vet Res Forum. 2012;3(4):251.
[49] Abidi SH, Ahmed K, Sherwani SK, et al. Synergy between antibiotics and natural agents results in increased antimicrobial activity against *Staphylococcus epidermidis*. J Infect Dev Ctries. 2015;9(9):925–929.
[50] Eshghi M, Vaghari H, Najian Y, et al. Microwave-assisted green synthesis of silver nanoparticles using Juglans regia leaf extract and evaluation of their Physico-chemical and antibacterial properties. Antibiotics. 2018;7(3):68–77.
[51] Sheikhlou K, Allahyari S, Sabouri S, et al. Walnut leaf extract-based green synthesis of selenium nanoparticles via microwave irradiation and their characteristics assessment. Open Agric. 2020;5 (1):227–235.
[52] Darvishi E, Kahrizi D, Arkan E. Comparison of different properties of zinc oxide nanoparticles synthesized by the green (using Juglans regia L. leaf extract) and chemical methods. J Mol Liq. 2019;286:110831.

[53] Pereira JA, Oliveira I, Sousa A, et al. Walnut (Juglans regia L.) leaves Phenolic compounds, antibacterial activity, and antioxidant potential of different cultivars. Food Chem Toxicol. 2007;45 (11):2287–2295.
[54] Zhang Z, Liao L, Moore J, et al. Antioxidant phenolic compounds from walnut kernels (Juglans regia L.). Food Chem. 2009;113(1):160–165.
[55] Chaleshtori RS, Chaleshtori FS, Rafieian M. Biological characterization of Iranian walnut (Juglans regia) leaves. Turk J Biol. 2011;35:635–939.
[56] Ayaz F, Şafak EK, Türkmen KE, et al. Assessment of antimicrobial, antibiofilm, and cytotoxic activities, and characterization of phenolic compounds of Origanum haussknechtii. J Food Meas Charact. 2021;15(5):4267–4276.
[57] Jayaprakash N, Suresh R, Rajalakshmi S, et al. One-step synthesis, characterization, photocatalytic and bio-medical applications of ZnO nanoplates. Mater Technol. 2020;35(2):112–124.
[58] Miri A, Mahdinejad N, Ebrahimy O, et al. Zinc oxide nanoparticles: biosynthesis, characterization, antifungal, and cytotoxic activity. Mater Sci Eng C. 2019;104:109981.
[59] Guo M, Ye L, Zhao L. Solid-state-grinding method to synthesize NiCoFe alloy/NiCoFe–OH nanosheets for asymmetric supercapacitor. J Alloys Compd. 2021;850:156787.
[60] Xue J, Yan H, Liu W, et al. Effect of Mn content on structural evolution and magnetic properties of ZnO Particles. J Supercond Nov Magn. 2020;34 (1):7–13.
[61] Siva N, Sakthi D, Ragupathy S, et al. Synthesis, structural, optical and photocatalytic behavior of Sn doped ZnO nanoparticles. Mater Sci Eng B. 2020;253:114497.
[62] Vijayaprasath G, Murugan R, Mahalingam T, et al. Enhancement of ferromagnetic property in rare earth neodymium-doped ZnO nanoparticles. Ceram Int. 2015;41(9):10607–10615.
[63] Fakhari S, Jamzad M, Kabiri Fard H. Green synthesis of zinc oxide nanoparticles: a comparison. Green Chem Lett Rev. 2019;12(1):19–24.
[64] Soares VA, Xavier MJ, Rodrigues ES, et al. Green synthesis of ZnO nanoparticles using whey as an effective chelating agent. Mater Lett. 2020;259:126853.
[65] Dinca V, Mocanu A, Isopencu G, et al. Biocompatible pure ZnO nanoparticles-3D bacterial cellulose biointerfaces with antibacterial properties. Arab J Chem. 2020;13(1):3521–3533.
[66] Zak AK, Majid WA, Mahmoudian MR, et al. Starch-stabilized synthesis of ZnO nanopowders at low temperature and optical properties study. Adv Powder Technol. 2013;24(3):618–624.
[67] Fakhari S, Jamzad M, Kabiri Fard H. Green synthesis of zinc oxide nanoparticles: a comparison. Green Chem Lett Rev. 2019;12(1):19–24.
[68] Kortum GFA. Reflectance spectroscopy: principles methods, applications, . New York; 1969.
[69] Parvin T, Keerthiraj N, Ibrahim IA, et al. Photocatalytic degradation of municipal wastewater and brilliant blue dye using hydrothermally synthesized surface-modified silver-doped ZnO designer particles. Int J Photoenergy. 2012;2012:1–8.
[70] Taufiq A, Ulya HN, Utomo J, et al. Structural, optical, and antifungal characters of zinc oxide nanoparticles prepared by Sol-gel method. J Phys Conf Ser. 2018;1093:012001.
[71] Darvishi E, Kahrizi D, Arkan E. Comparison of different properties of zinc oxide nanoparticles synthesized by the green (using Juglans regia L. leaf extract) and chemical methods. J Mol Liq. 2019;286:110831.
[72] Arvanag FM, Bayrami A, Habibi-Yangjeh A, et al. A comprehensive study on antidiabetic and antibacterial activities of ZnO nanoparticles biosynthesized using Silybum marianum L seed extract. Mater Sci Eng C. 2019;97:397–405.
[73] Abdulkhair BY, Salih ME, Elamin NY, et al. Simplistic synthesis and enhanced photocatalytic performance of spherical ZnO nanoparticles prepared from arabinose solution. Z Naturforschung A. 2019;74:937–944.
[74] Gupta M, Tomar RS, Kaushik S, et al. Effective antimicrobial activity of green ZnO nanoparticles of Catharanthus roseus. Front Microbiol. 2018;9:2030.
[75] Jalal M, Ansari MA, Ali SG, et al. Anticandidal activity of bioinspired ZnO NPs: effect on growth, cell morphology and key virulence attributes of Candida species. Artif Cells Nanomed Biotechnol. 2018;46 (sup1):912–925.
[76] Shoeb M, Singh BR, Khan JA, et al. ROS-dependent anticandidal activity of zinc oxide nanoparticles synthesized by using egg albumen as a biotemplate. Adv Nat Sci Nanosci Nanotechnol. 2013;4(3):035015.